Fuzzy adaptive singular value decomposition cubature Kalman filtering algorithm for lithium-ion battery state-of-charge estimation.

YANG, X., WANG, S., XU, W., QIAO, J., YU, C. and FERNANDEZ, C.

2022

International Journal of Circuit Theory and Applications

Fuzzy adaptive singular value decomposition cubature Kalman filtering algorithm for Lithium-ion battery state-of-charge estimation

Journal:	*International Journal of Circuit Theory and Applications*
Manuscript ID	CTA-21-0518.R2
Wiley - Manuscript type:	Original Papers
Date Submitted by the Author:	04-Oct-2021
Complete List of Authors:	Yang, Xiao; Southwest University of Science and Technology, Wang, Shunli ; Southwest University of Science and Technology, School of Information Engineering Xu, Wenhua; Southwest University of Science and Technology Qiao, Jialu; Southwest University of Science and Technology, ; Yu, Chunmei; Southwest University of Science and Technology Fernandez, Carlos; Robert Gordon University
Keyword:	lithium-ion battery, state of charge, convergence speed, fuzzy adaptive algorithm, singular value decomposition, double internal resistance

Fuzzy adaptive singular value decomposition cubature Kalman filtering algorithm for Lithium-ion battery state-of-charge estimation

Xiao Yang[1], Shunli Wang[1*], Wenhua Xu[1], Jialu Qiao[1], Chunmei Yu[1], Carlos Fernandez[2]

[1]School of Information Engineering, Southwest University of Science and Technology, Mianyang 621010, China; [2]School of Pharmacy and Life Sciences, Robert Gordon University, Aberdeen AB10-7GJ, UK.

Abstract: To solve the problem of the slow convergence speed for the battery state-of-charge estimation of cubature Kalman filter algorithm, the ternary lithium-ion battery is taken as the research object, and an algorithm combining the fuzzy self-adaptation and singular value decomposition cubature Kalman filtering is proposed. The algorithm takes the system innovation and its change rate as the fuzzy input, and the output as the adjustment factor, which is used to adjust the process noise covariance matrix *R*. The Kalman gain is adjusted through the fuzzy control of *R*. To ensure the stability of the algorithm in the calculation process, the singular value decomposition is applied to cubature Kalman algorithm. Then, a second-order RC equivalent circuit model with double internal resistance is built and tested under different conditions to verify the rationality of the improved algorithm. The verification results show that under the simple condition， the convergence speed of the proposed algorithm in the different initial state-of-charge values increased by 40.00% and 25.00%, respectively, the maximum estimation error of the state-of-charge is 2.52% and 2.51%, the Mean Absolute Error is 0.816 and 0.880%, the Root Mean Square Error is respectively 1.276% and 1.380. When the initial state-of-charge value is 0.8, the convergence speed in the complex condition is increased by about 30.00%, the maximum estimation result error, Mean Absolute Error and Root Mean Square Error are 2.21%, 0.222%, and 1.327%, respectively. When the initial state-of-charge value is 0.6， the convergence speed in the complex condition is increased by about 10.00%, the maximum estimation result error, Mean Absolute Error, and Root Mean Square Error are 2.72%, 0.941%, and 1.327%, respectively. Without reducing the estimation accuracy, the improved algorithm can significantly increase the convergence speed of predictive value tracking, which provides a theoretical basis for the wide application of lithium-ion batteries.

Keywords: lithium-ion battery; state-of-charge; convergence speed; fuzzy adaptive algorithm; singular value decomposition; double internal resistance

***Corresponding author**: Shun-Li Wang. Tel: +86-15884655563. E-mail address: 497420789@qq.com.

1. Introduction

With the rapid economic development, the problems of resource shortages and environmental pollution are increasingly serious [1-4], the green energy and environmental protection development have become common concerns of all countries in the world [5-8]. Due to the advantages of high energy density, long service life, and low environmental pollution, lithium-ion batteries are widely used in new energy vehicles, special robots, and aerospace fields. With the continuous expansion of its application range, the research on battery management systems (BMS) has received increasing attention for the reliable operation of lithium-ion batteries [9-13]. In the BMS, the accurate estimation of the state-of-charge (SOC) is very important, which is a key factor for safe charging-discharging and accurate life estimation of the battery pack [14-17].

Lithium-ion batteries mostly work in complex environments [18-22], these working environments and sensor measurement errors will increase the difficulty of accurate SOC estimation [23-27]. As a state variable, SOC cannot be directly measured by sensors, but can only be obtained through the calculation of related parameters. The methods for SOC estimation can be roughly divided into ampere-hour (Ah) integration, open-circuit voltage (OCV) method, model-based estimation method, and the way based on data-driven. The Ah integration is simple in principle and easy to implement, but as an open-loop estimation system, it cannot realize the correction of the initial value, and the error will continue to accumulate. Common improvement methods for the Ah algorithm include the combination of Ah integration and adaptive extended Kalman filter (EKF) [28]. In this method, the adaptive EKF algorithm is used to obtain the initial SOC value, and switch to the Ah algorithm for SOC estimation when the estimated value converges. If the estimation error reaches the set value, it switches to the adaptive EKF algorithm for SOC estimation again. This algorithm effectively avoids the error accumulation of Ah and the correction of the initial error, which reduces the estimation time of the adaptive EKF algorithm, obtains a higher SOC estimation accuracy, and has strong practicability. The OCV method estimates the SOC value through the function curve of the OCV and SOC value, however, it is difficult to obtain the OCV value of the lithium-ion battery in actual working conditions, so it is impossible to directly apply this method to engineering practice. Wang et al. proposed a fusion OCV estimation method [29], which obtains the fused OCV data through the first-order backward differential integration of the small current test results, and fits the data through a neural network to obtain the OCV-SOC curve. This method reduces the influence of the battery polarization effect and has a high SOC estimation accuracy.

There are many model-based estimation methods, and the most widely used equivalent circuit models are Thevenin equivalent model, second-order RC equivalent model, etc. After the equivalent model of the battery is established, parameter identification is performed online or offline, and then, related algorithms are used to estimate the SOC. Jiang Cong et al. proposed an adaptive square root extended Kalman SOC estimation method based on the Thevenin model [30]. This method combines the adaptive algorithm with the square root algorithm, which improves the accuracy of SOC estimation while maintaining the stability of the calculation process, and it has good results at different temperatures. Peng N et al. proposed a SOC estimation method based on online parameter identification and improved adaptive dual unscented Kalman filter (ADUKF) algorithm [31], in which the singular value decomposition (SVD) algorithm is used to solve the problem of divergence of the noise covariance matrix, then, two UKF algorithms are used to realize the co-estimation of parameters and SOC, while an adaptive algorithm is adopted to improve the estimation accuracy. The verification results show that the SOC estimation accuracy of this method is much higher than that of the ordinary DUKF. The data-driven SOC estimation method does not rely on an accurate battery model, it has great advantages when the system model is difficult to describe. Common data-driven methods include artificial neural network (ANN), support vector machine (SVM), and extreme learning machine (ELM). For example, Ma, L et al. proposed a method for co-estimation of SOC and state-of-energy (SOE) based on long short term memory (LSTM) neural network[32], in which good estimation results can be obtained under different working conditions.

Aiming at the goal of shortening the convergence time of the cubature Kalman filtering algorithm (CKF), an algorithm that combines the fuzzy adaptive algorithm and SVD method with CKF is proposed to estimate the lithium-ion battery SOC, and a second-order RC model with double internal resistance is established. On the premise of ensuring the stability of the algorithm and accuracy of the estimation, this method shortens the convergence time of the SOC estimation. In addition, the application of double internal resistance can significantly improve the accuracy of the second-order RC model.

2. Mathematical analysis

2.1. Second-order RC equivalent circuit with double internal resistance modeling

A reasonable battery equivalent model is the basis for accurate SOC estimation. Common lithium-ion battery equivalent models include Thevenin equivalent model, PNGV model, and second-order RC model [33-38]. Taking into account the requirements of battery simulation accuracy and the principle of minimizing the amount of calculation, a second-order RC equivalent model is selected to perform equivalent simulations of lithium-ion batteries. For the internal resistance of the battery is different during charging and discharging, the internal resistance of the battery for charging and discharging is calculated separately to form a double internal resistance second-order RC model [39-41]. The equivalent circuit is shown in Figure 1.

[Insert Figure 1]

Figure 1. The second-order RC equivalent model of lithium-ion battery with double internal resistance

In Figure 1, U_{OC} represents the open-circuit voltage, R_1 and R_2 are polarization resistances, C_1 and C_2 are polarization capacitances, the R_1C_1 loop is used for the concentration polarization phenomenon of the equivalent circuit, and to characterize the process of rapid voltage changes when the current changes suddenly. The R_2C_2 loop is used for the electrochemical polarization phenomenon of the equivalent circuit, and to characterize the process of slow voltage changes. U_L is the terminal voltage of the circuit, $I(t)$ is the internal current of the battery, R_{01} and R_{02} represent the internal resistance of the battery during discharging and charging, respectively. Taking the discharge direction as the reference, the KVL equations are shown in Equation (1).

$$\begin{cases} U_L = U_{OC} - U_0 - U_1 - U_2 \\ \dfrac{dU_1}{dt} = \dfrac{I}{C_1} - \dfrac{U_1}{R_1 C_1} \\ \dfrac{dU_2}{dt} = \dfrac{I}{C_2} - \dfrac{U_2}{R_2 C_2} \end{cases} \Leftarrow \begin{cases} U_0 = IR_{01}, (disch\arg e) \\ U_0 = -IR_{02}, (ch\arg e) \end{cases} \tag{1}$$

In Equation (1), U_1 and U_2 represent the voltage across R_1C_1 and R_2C_2, respectively. Taking the state variable of the circuit as $x=[SOC, U_1, U_2]^T$, and the terminal voltage U_L as the observation variable, the state equation and observation equation of the model can be obtained as shown in Equation (2).

$$\begin{cases} \begin{bmatrix} SOC_{k+1} \\ U_{1,k+1} \\ U_{2,k+1} \end{bmatrix} = \begin{bmatrix} 1 & 0 & 0 \\ 0 & e^{\Delta t/\tau_1} & 0 \\ 0 & 0 & e^{\Delta t/\tau_2} \end{bmatrix} \begin{bmatrix} SOC_k \\ U_{1,k} \\ U_{2,k} \end{bmatrix} + \begin{bmatrix} -\dfrac{\eta \Delta t}{Q_N} \\ R_1\left(1 - e^{T/\tau_1}\right) \\ R_2\left(1 - e^{T/\tau_2}\right) \end{bmatrix} I_k + w_k \Leftarrow \begin{cases} \tau_1 = R_1 C_1 \\ \tau_2 = R_2 C_2 \end{cases} \\ U_{L,k+1} = \begin{bmatrix} \dfrac{\partial U_{OC}}{\partial SOC} & -1 & -1 \end{bmatrix} \begin{bmatrix} SOC_k \\ U_{1,k} \\ U_{1,2} \end{bmatrix} - U_0 + v_k \quad \Leftarrow \begin{cases} U_0 = IR_{01}, (disch\arg e) \\ U_0 = -IR_{02}, (ch\arg e) \end{cases} \end{cases} \tag{2}$$

In Equation (2), Q_N is the actual capacity of the battery, Δt is the sampling time, τ is the time constant, w_k and v_k respectively represent the system observation error and measurement error, η is the Coulomb efficiency, which is generally equal to one.

2.2. Parameter identification of the equivalent model of lithium-ion battery

High-precision model parameters are the prerequisite for accurate lithium-ion batteries SOC estimation [42, 43]. With the method of curve fitting, the Hybrid Pulse Power Characteristic (HPPC) condition data is selected for model parameter identification. Due to the inconsistency of model parameters in the charging and discharging process, to improve the accuracy of the model, it is necessary to identify the two processes separately. Taking the parameter identification of the discharge process as an example, the voltage and current curves of one cycle for HPPC condition are shown in Figure 2.

[Insert Figure 2]

Figure 2. The current and voltage curve of the HPPC working condition

When the battery is charged and discharged in the HPPC condition, the instantaneous change of current will cause the change of the internal resistance terminal voltage of the battery, that is, the sudden changes in the voltage curve of the AB and CD segments in Figure 2 is caused by the internal resistance of the battery. To improve the accuracy, the internal resistance of the two voltages is calculated separately, and the average value is taken as the final result. The calculation process is shown in Equation (3).

$$R_{01} = \frac{U_A - U_B + U_D - U_C}{2I} \tag{3}$$

The DE part in Figure 2 shows the discharging process of the polarizing capacitor to the polarizing resistor, and $I(t)$ is equal to zero, which is a zero-input response. For a simplified calculation, this curve is used for fitting to obtain the relevant parameter values. The response function of DE segment and its simplified expression are shown in Equation (4).

$$\begin{cases} U_L = U_{OC} - IR_1 e^{\frac{-t}{\tau 1}} - IR_2 e^{\frac{-t}{\tau 2}} \\ U_L = U_{OC} - ae^{-bt} - ce^{-dt} \end{cases} \tag{4}$$

According to the corresponding relationship between the parameters and coefficients in Equation (4), the relevant parameters of the model can be obtained. Taking into account the hysteresis voltage characteristics of lithium-ion batteries, the open-circuit voltage during the charging and discharge process are respectively fitted and averaged. The open-circuit voltage curves are shown in Figure 3.

[Insert Figure 3]

Figure 3. The fitting curve of the U_{OC}-SOC

In Figure 3, U_{OC1} is the OCV curve of the charging process, U_{OC2} is that of the discharging process, and U_{OC3} is the mean voltage fitting curve of the charging and discharging. It can be seen from the figure that the difference in OCV between charge and discharge is small, so the average value of the two curves is selected as the final fitting result.

2.3. Fuzzy adaptive algorithm

Lithium-ion batteries mostly work in complex environmental conditions. For the influence of environmental factors, the statistical characteristics of the observation noise will keep changing, which leads to the continuous change of the observation noise covariance matrix R [44-47]. To improve the convergence speed of the CKF, a fuzzy adaptive algorithm is introduced. The innovation e_k and its rate of change Δe_k are selected as the input of the fuzzy controller, and the adjustment factor α of R as the output. The input expressions of the system are shown in Equation (5).

$$\begin{cases} e_k = y_k - y_k^* \\ \nabla e_k = e_k - e_{k-1} \end{cases} \tag{5}$$

In Equation (5), y_k represents the measured value of the terminal voltage, y_k* represents the estimated value of the terminal voltage. In the fuzzy adaptive system, under ideal conditions, the system innovation is zero, when the innovation and its rate of change are large, the output value will increase, and thereby the Kalman gain is reduced. When the innovation and its rate of change are small, the output value decreases, making the Kalman gain larger and increasing the proportion of the measured value, to achieve the purpose of making the algorithm stable and converging quickly. The theoretical residual covariance matrix expression after introducing the adjustment factor is shown in Equation (6).

$$P_{zz,k|k-1} = \frac{1}{2n}\sum_{i=1}^{2n}\left(z_{i,k|k-1}z_{i,k|k-1}^{T} - \hat{z}_{i,k|k-1}\hat{z}_{i,k|k-1}^{T}\right) + \alpha R \tag{6}$$

It is assumed that the innovation interval is [-0.04, 0.04], and divide it into six segments: very small, small, medium, big, and very big. The domain of innovation change rate is set as [-0.035, 0.035], which is divided as small, medium, big, and very big. The membership functions of e_k and Δe_k are shown in Figure 4.

[Insert Figure 4(a)] [Insert Figure 4(b)]

(a) The membership function graph of e_k (b) The membership function graph of Δe_k

Figure 4. The membership function graph of the input variable

Assuming that the output domain of the fuzzy system is [0.2, 2], the output of the fuzzy system is divided into five intervals of very small, small, medium, big, and very big according to the actual situation, the domain of α is shown in Figure 5.

[Insert Figure 5]

Figure 5. The membership function graph of the output variable

Reasonable fuzzy rules can reduce the amount of calculation [48, 49]. The larger the number of fuzzy rules, the greater the amount of calculation, considering the trade-off between computational complexity and accuracy, the fuzzy rules are established as shown in Table 1.

[Insert Table 1]

Table 1. The table of fuzzy rule

A logical defuzzification method is very important for the fuzzy control system. Common methods include the membership average method, the area centroid method, and the area equal division method [50]. To obtain good output results, the area centroid method is chosen for defuzzification. The fuzzy input-output surface is shown in

Figure 6.

[Insert Figure 6]

Figure 6. The graph of fuzzy rules

2.4. Fuzzy adaptive singular value decomposition cubature Kalman filter algorithm

For the state covariance matrix is prone to be non-positive definite when calculates the cubature point in the CKF algorithm, the SVD method is introduced [51, 52]. This method does not need to meet the condition that the covariance matrix must be positive definite, which can make the algorithm more stable.

The SOC estimation based on fuzzy adaptive SVD-CKF (FASVD-CKF) can be divided into three parts, namely initialization, time update, and measurement update. The initial state variables and value of the error covariance matrix are defined as shown in Equation (7).

$$\begin{cases} \hat{x}_{0|0} = E\left(x_0\right) \\ P_0 = E\left[\left(x_0 - \hat{x}_0\right)\left(x_0 - \hat{x}_0\right)^T\right] \end{cases} \tag{7}$$

In Equation (7), E represents the expectation of the variable. The time update process includes the prediction of state and error covariance matrix through the cubature point calculation. The calculation process is shown in Equation (8).

$$\begin{cases} P_{k-1|k-1} = U_{k-1} S_{k-1} V_{k-1}^T \\ x_{i,k-1|k-1} = U_{k-1}\sqrt{S_i}\,\xi_i + x_{k-1|k-1} \\ x_{i,k|k-1}^* = f\left(x_{i,k-1|k-1}, u_{k-1}\right) \\ \hat{x}_{k|k-1} = \dfrac{1}{2n}\sum\limits_{i=1}^{2n} x_{k|k-1}^* \\ P_{k|k-1} = \dfrac{1}{2n}\sum\limits_{i=1}^{2n} x_{k|k-1}^* x_{k|k-1}^{*}{}^{T} - \hat{x}_{k|k-1}\hat{x}_{k|k-1}^T \end{cases} \tag{8}$$

The measurement update process mainly includes the calculation of auto-covariance and cross-covariance matrices and obtains the Kalman gain, state variable estimates, and state estimation error covariance matrix. The calculations of the self-covariance and the cross-covariance matrix are shown in Equation (9).

$$\begin{cases} P_{k|k-1} = U_{k-1}^{*} S_{k-1}^{*} \left(V_{k-1}^{*}\right)^{T} \\ x_{i,k|k-1} = U_{k-1}^{*} \sqrt{S_{k-1}^{*}} \xi_{i} + \hat{x}_{k|k-1} \\ P_{zz,k|k-1} = \dfrac{1}{2n} \sum_{i=1}^{2n} \left(z_{i,k|k-1} z_{i,k|k-1}^{T} - \hat{z}_{i,k|k-1} \hat{z}_{i,k|k-1}^{T} \right) + \alpha R \\ P_{xz,k|k-1} = \dfrac{1}{2n} \sum_{i=1}^{2n} \left(x_{i,k|k-1} z_{i,k|k-1}^{T} - \hat{x}_{i,k|k-1} \hat{z}_{i,k|k-1}^{T} \right) \end{cases} \Leftarrow \begin{cases} z_{k|k-1} = h\left(x_{k|k-1}\right) \\ \hat{z}_{k|k-1} = \dfrac{1}{2n} \sum_{1}^{2n} z_{k|k-1} \end{cases} \tag{9}$$

The Kalman gain can be calculated by the auto-covariance and cross-covariance matrices. The expressions of Kalman gain, state variable estimated value, and state estimation error covariance matrix are shown in Equation (10).

$$\begin{cases} K_{k} = P_{xz,k|k-1} / P_{zz,k|k-1} \\ \hat{x}_{k|k} = \hat{x}_{k|k-1} + K_{k} \left(z_{k} - \hat{z}_{k|k-1} \right) \\ P_{k|k} = P_{k|k-1} - K_{k} P_{zz,k|k-1} K_{k}^{T} \end{cases} \tag{10}$$

Equations (7) to (10) are a complete SOC estimation process. At this point, the state estimation at time k is completed, and the time point $k=k+1$ is set to realize the state estimation at the next time. The flow chart of SOC estimation based on FASVD-CKF is shown in Figure 7.

[Insert Figure 7]

Figure 7. The flow chart of FASVD-CKF

Based on the cubature criterion, the CKF algorithm approximates the state mean and covariance of the nonlinear system through $2n$ cubature points with the same weight. This can avoid the process of linearizing the nonlinear system, and theoretically has a higher estimation accuracy than the EKF algorithm. The fuzzy adaptive algorithm improves the convergence speed of the CKF, and the application of the SVD algorithm solves the problem of instability of the state estimation covariance matrix during the operation.

3. Analysis of experimental results

A ternary lithium-ion battery with a rated capacity of 70Ah is taken as the experimental object. To obtain relevant experimental data, an experimental platform is built with the BTS200-100-104 battery test device and temperature control equipment. The platform is shown in Figure 8.

[Insert Figure 8]

Figure 8. Experimental platform

All data are carried out at a constant temperature of 35°C. Measured with the cyclic discharge experiment, the actual capacity of the experimental battery is 68.27Ah.

3.1 Analysis of parameter identification results

The curve fitting method is used to identify the parameters of the equivalent model. The average curve expression of the open-circuit voltage function obtained by the charge and discharge of HPPC test is shown in Equation (11).

$$\begin{aligned} U_{OC} &= 2.269*SOC^5 - 9.252*SOC^4 + 13.51*SOC^3 - 8.073*SOC^2 + 2.45*SOC + \\ &3.275 + 0.5*\left(-3.011*SOC^4 + 7.233*SOC^3 - 5.264*SOC^2 + 1.915*SOC + 3.307\right) \end{aligned} \quad (11)$$

Taking into account the differences in model parameters during the charging and discharging process, parameter identification is carried out separately during the two processes. The identification results are shown in Table 2 and Table 3.

Table 2. Model parameters for the discharging process

[Insert Table 2]

Table 3. Model parameters for the charging process

[Insert Table 3]

To simplify the calculation process, R_{01} and R_{02} are the average values under different SOC values during the discharge and charge process, respectively. For R_1, R_2, C_1, and C_2, all charge-discharge data are selected and the average value is taken as the final result. The accuracy of the model is verified under HPPC condition, and the results are shown in Figure 9.

[Insert Figure 9 (a)]

(a) The voltage comparison of HPPC working condition

[Insert Figure 9 (b)]

(b) Identification error of HPPC working condition

Figure 9. Comparison of model voltage effect

In Figure 9(a), UL1 and UL2 represent the actual voltage and analog voltage respectively. It can be seen from Figure 9(b) that the maximum error of the analog voltage is 0.0266V, overall, the error is small and fluctuates in a small range. The adopted method can obtain high-precision model parameters, which lays the foundation for the accurate estimation of the SOC value.

3.2 Analysis of experimental results of DST working condition

To verify the SOC estimation effect of the proposed method, an experimental analysis is carried out under the dynamic stress test (DST) condition. This condition includes charging, discharging, and shelving processes of different lengths of time, which can effectively simulate the actual working conditions of lithium-ion batteries.

The process noise covariance matrix is set as Q = diag (10^{-6} 10^{-6} 10^{-6}), and the observed noise covariance matrix R is 0.05. The initial value of actual SOC is 1, and the initial SOC value of the other three algorithms is 0.8. The voltage curve of DST and the SOC estimation results of different algorithms are shown in Figure 10.

[Insert Figure 10 (a)]

(a) The voltage curve of DST condition

[Insert Figure 10 (b)]

(b) SOC estimation under DST condition

[Insert Figure 10 (c)]

[Insert Figure 10 (d)]

(c) The error of SOC estimation under DST condition

(d) Convergence process of different algorithms under DST condition

Figure 10. The data and SOC estimation results of the DST condition when $SOC_0 = 0.8$

In Figure 10, S0 represents the SOC reference value, S1 is the SOC estimation result of the EKF algorithm, S2 and S3 are the SOC values estimated by the CKF algorithm and FASVD-CKF algorithm, respectively. Err1~Err3 are the estimation errors corresponding to S1, S2, and S3. It can be seen from Figure 10 (c) that all three algorithms have large estimation errors at the end of discharge, which is caused by the severe chemical reaction inside the battery. In the stable discharge stage, the accuracy of the estimation results of the CKF and FASVD-CKF algorithms is almost the same, the maximum errors of SOC estimation for them are about 2.52%, and the maximum error for that of the EKF algorithm is about 2.11%. In Figure 10 (d), the convergence time of the FASVD-CKF, CKF, and EKF is about 30 s, 50 s, and 65 s, respectively. Compared with CKF, the convergence time of the improved algorithm is shortened by about 40.00%, indicating that the introduction of the fuzzy adaptive algorithm can improve the convergence speed of the algorithm SOC estimation.

For a more intuitive comparison of the three algorithms SOC estimation results, the Mean Absolute Error (MAE) and Root Mean Square Error (RMSE) of the estimation results are compared and analyzed as shown in Table 4.

Table 4 Comparison of performance indicators of various algorithms under DST operating conditions

[Insert Table 4]

The MAE of the FASVD-CKF algorithm is 0.816%, which is smaller than that of the CKF and EKF algorithms. With a small difference, the RMSE value of FASVD-CKF is between the data of EKF and CKF algorithms. In Table 4 and Figure 10, it can be seen that the FASVD-CKF can significantly improve the convergence speed, and the introduction of the fuzzy adaptive algorithm does not significantly reduce the accuracy of the CKF algorithm. In general, the algorithm has high stability and there is no divergence in the SOC estimation process, which proves that the SVD algorithm can effectively preserve the stability of the improved algorithm.

To further verify the estimation effect of the proposed algorithm under different initial SOC conditions, the initial SOC value is set to 0.7, and other conditions are consistent with the previous ones. The estimation results are shown in Figure 11.

[Insert Figure 11 (a)]

[Insert Figure 11 (b)]

(a) Convergence process of different algorithms under DST condition

(b) The error of SOC estimation under DST condition

Figure 11. The SOC estimation result under DST condition when $SOC_0 = 0.7$

Figure 11(a) shows the convergence process of the three algorithms, and the legend is consistent with Figure 10. In Figure 11(a), the convergence time of S1, S2 is 120 s and 60 s respectively. The time of S3 is about 45 s, which is about 25% shorter than that of S2. It means that the fuzzy adaptive algorithm can still improve the convergence speed of the algorithm in different SOC initial values. In Figure 11(b), Err2 and Err3 show a high degree of overlap, the maximum SOC estimation error of the two algorithms is about 2.51% except for the end of discharge, and the maximum error of the EKF is about 2.23%. The MAE and RMSE comparisons of the three algorithms are shown in Table 5.

Table 5. Comparison of performance indicators of various algorithms under DST operating conditions

[Insert Table 5]

In Table 5, the MAE of the improved algorithm is 0.880%, which is slightly smaller than that of EKF, but greater than the value of the CKF algorithm, indicating that the estimation error of the FASVD-CKF algorithm is smaller than that of EKF. Compared with CKF, there is almost the same SOC estimation accuracy of FASVD-CKF. The RMSE value of the improved algorithm is 1.380%, which is slightly larger than that of the other two algorithms. The error fluctuation range of FASVD-CKF is larger than that of EKF and CKF.

Compared with the CKF and EKF, the SOC estimation error of the FASVD-CKF algorithm increases slightly, but the final estimation result still has a higher estimation accuracy, so it is feasible to improve the convergence speed of the CKF algorithm SOC estimation by the fuzzy adaptive algorithm.

3.3 *Analysis of experimental results of BBDST working condition*

Lithium-ion batteries are widely used in many fields such as energy storage, new energy vehicles, and aerospace. To further verify the SOC estimation effect of the FASVD-CKF algorithm under complex working conditions, the experimental verification is carried out under Beijing Bus Dynamic Stress Test (BBDST) condition. It is designed to reduce the power according to the actual operating conditions of the car, which includes 19 working steps such as starting, coasting, braking, and rapid acceleration, so it can effectively simulate the actual working conditions of the battery.

The process noise covariance is set as Q = diag (10^{-6} 10^{-6} 10^{-6}), the observed noise covariance is R = 0.05, and the initial value of SOC in each algorithm is 0.08. The BBDST working condition voltage curve and SOC estimation results are shown in Figure 12.

[Insert Figure 12 (a)]

(a) The voltage curve of BBDST condition

[Insert Figure 12 (b)]

(b) SOC estimation under BBDST condition

[Insert Figure 12 (c)]

(c) The error of SOC estimation under BBDST condition

[Insert Figure 12 (d)]

(d) Convergence process of different algorithms under BBDST condition

Figure 12. SOC estimation results and errors of BBDST experimental when SOC_0 = 0.8

In Figure 12, S0 represents the actual SOC value, S1 represents the SOC estimation value based on the EKF algorithm, S2 is the SOC estimation value based on the CKF algorithm, S3 is the SOC estimation result based on the FASVD-CKF algorithm, and Err1~Err3 are S1~S3 corresponding SOC estimation error, respectively. It can be seen from Figure 12 (b) that the SOC estimation curves of the CKF and the FASVD-CKF algorithm have a higher degree of overlap, and the estimation results of the EKF are slightly different from the two. In Figure 12 (c), Err2 and Err3 are highly consistent in the stable stage of SOC estimation with a maximum error of 2.21%. Overall, the fluctuation range for Err3 is small, while Err1 is somewhat different from the two Errs. For the fierce internal chemical reaction of the battery, at the end of discharge, the accuracy of the SOC estimation is reduced. In Figure 12 (d), the convergence time of S1 and S2 is about 60 s and 50 s， respectively， and the time of S3 is about 35s, which is 30.00% higher than the convergence speed of S2. The convergence speed of S3 is faster than that of the other two algorithms, so the FASVD-CKF algorithm still has good results under complex working conditions. Therefore, the fuzzy adaptive algorithm can improve the convergence speed of the algorithm effectively. To further visually compare the SOC estimation effects of the three algorithms, the MAE and RMSE of the algorithms are compared as shown in Table 6.

Table 6. Comparison of performance indicators of various algorithms under BBDST operating conditions

[Insert Table 6]

In Table 6, the MAE and RMSE values of the FASVD-CKF algorithm are 0.222% and 1.327%, respectively, which are slightly different from the CKF algorithm and smaller than the values of the EKF algorithm. Combining Table 6 with Figure 12, it can be seen that the fuzzy adaptive algorithm can effectively improve the convergence effect of the CKF algorithm without reducing the accuracy of SOC estimation. In the entire estimation process, except for the divergence of the algorithm due to the chemical reaction inside the battery at the end of discharge, the other parts of the curve are relatively stable, indicating that the SVD algorithm can still maintain the stability of the algorithm under complex working conditions. To verify the estimation effect of the FASVD-CKF algorithm under different initial values, the SOC_0 is 0.6, and other parameters remain unchanged, the estimation results are shown in Figure 13.

[Insert Figure 13 (a)] [Insert Figure 13 (b)]

(a) Convergence process of different algorithms under BBDST condition

(b) The error of SOC estimation under BBDST condition

Figure 13. SOC estimation results under BBDST condition when $SOC_0 = 0.6$

Figure 13 (a) shows the convergence effects of the three algorithms, S0 is the reference value, S1 is the SOC estimation result of the EKF algorithm, S2, S3 are the SOC estimation results of the CKF and FASVD-CKF algorithms, respectively. The convergence time of S1 and S2 is about 200 s, and the time of S3 is about 180 s, which means that the convergence speed of the improved algorithm is increased by 10.00%. Compared with S1 and S2, S3 has a better convergence effect, and the FASVD-CKF still has a good convergence effect when estimating the SOC of lithium-ion batteries under complicated working conditions. Figure 13 (b) shows the SOC estimation error curve, and Err1~Err3 are the SOC estimation errors corresponding to S1~S3, respectively. It can be seen from the figure that the error curves of Err2 and Err3 almost overlap, and there is a slight difference between Err1 and the other two errors. The comparison results of MAE and RMSE of the three results are shown in Table 7.

Table 7. Comparison of performance indicators of various algorithms under BBDST operating conditions

[Insert Table 7]

It can be seen from Table 7 that there is no significant difference between the estimation effects of CKF and FASVD-CKF algorithms, and the estimation results of both algorithms are better than that of EKF. It is feasible to improve the convergence speed of the algorithm through the fuzzy adaptive algorithm. Except for the part at the end of the discharge, the algorithm stability is relatively high, therefore, the SVD algorithm can effectively ensure the stability of the algorithm.

Compared with the traditional CKF algorithm, the convergence speed of the FASVD-CKF algorithm is improved by the introduction of the fuzzy adaptive algorithm, through the SVD algorithm, the stability of the algorithm is guaranteed. However, in the fuzzy adaptive algorithm, the more fuzzy rules, the greater the computational complexity, which increases the time required for the entire process, and it can be further improved.

4. Conclusions

The real-time accurate estimation of SOC provides an important guarantee for the safe operation of the BMS, and it is also a hot and important topic of research. Aiming at improving the convergence speed of the SOC estimation, the FASVD-CKF algorithm is proposed based on the double internal resistance model, and it is experimentally verified through DST and BBDST conditions under different initial states. The verification results show that it is feasible to construct a fuzzy system that uses innovation and its change rate as input and output coefficients to adjust R to improve the convergence speed of the algorithm. In the DST condition, when the initial SOC value is 0.8, the convergence time of the FASVD-CKF algorithm under DST working condition is 30 s, the maximum estimation error is 2.52%, and the MAE and RMSE are 0.816% and 1.216% respectively. Compared with the estimation results of the CKF algorithm, the convergence speed of the proposed algorithm is increased by about 40.00% while the accuracy remains almost unchanged. When the initial SOC value is 0.7, the verification results are completely consistent with the initial SOC value of 0.8. Under the BBDST condition, when the initial SOC value is 0.8, the convergence time is 35 s, which is 30.00% faster than that of the CKF algorithm. The maximum estimation error, the MAE and RMSE values are 2.21%, 0.222%, and 1.327%, respectively. When the initial SOC value is 0.6, almost consistent verification results can be obtained. Overall, the accuracy of the algorithm is high, and the SVD algorithm can effectively ensure the stability of the algorithm. The FASVD-CKF algorithm has a high convergence speed under the premise of ensuring accuracy, which provides a basis for optimizing the battery management system, and is of positive significance to the application and promotion of lithium-ion batteries.

The Fuzzy rules will increase the computational complexity of the algorithm, which can be further optimized. In the future, based on this algorithm, a dual-adaptive algorithm will be proposed to reduce the computational complexity, and achieve the improvement of state estimation accuracy and convergence speed.

Acknowledgments

The work was supported by National Natural Science Foundation of China (No. 61801407), China Scholarship Council (No. 201908515099), Fund of Robot Technology Used for Special Environment Key Laboratory of Sichuan Province (No. 18kftk03), and Natural Science Foundation of Southwest University of Science and Technology (No.17zx7110, 18zx7145).

References

1. Xu, W., et al., *A novel adaptive dual extended Kalman filtering algorithm for the Li-ion battery state of charge and state of health co-estimation.* International Journal of Energy Research, 2021.
2. Wang, S.-L., et al., *Adaptive State-of-Charge Estimation Method for an Aeronautical Lithium-ion Battery Pack Based on a Reduced Particle-unscented Kalman Filter.* Journal of Power Electronics, 2018. **18**(4): p. 1127-1139.
3. Chen, Z., et al., *Online state of charge estimation of Li-ion battery based on an improved unscented Kalman filter approach.* Applied Mathematical Modelling, 2019. **70**: p. 532-544.
4. Meng, J.H., et al., *Low-complexity online estimation for LiFePO4 battery state of charge in electric vehicles.* Journal of Power Sources, 2018. **395**: p. 280-288.
5. Xin, X., et al., *A Novel State of Charge Estimation Method for Ternary Lithium Batteries Based on System Function and Extended Kalman Filter.* International Journal of Electrochemical Science, 2020. **15**(3): p. 2226-2242.
6. Shi, H., et al., *A Novel Dual Correction Extended Kalman Filtering Algorithm for The State of Charge Real-Time Estimation of Packing Lithium-Ion Batteries.* International Journal of Electrochemical Science, 2020. **15**(12): p. 12706-12723.
7. Liu, M., et al., *A high-order state-of-charge estimation model by cubature particle filter.* Measurement, 2019. **146**: p. 35-42.
8. Wang, S.-L., et al., *An adaptive working state iterative calculation method of the power battery by using the improved Kalman filtering algorithm and considering the relaxation effect.* Journal of Power Sources, 2019. **428**: p. 67-75.
9. Ji, H., et al., *State of health prediction model based on internal resistance.* International Journal of Energy Research, 2020. **44**(8): p. 6502-6510.
10. Yang, F., et al., *State-of-Charge Estimation of Lithium-Ion Batteries via Long Short-Term Memory Network.* Ieee Access, 2019. **7**: p. 53792-53799.
11. Zhang, N., et al., *A Novel Method for Estimating State-of-Charge in Power Batteries for Electric Vehicles.* International Journal of Precision Engineering and Manufacturing, 2019. **20**(5): p. 845-852.
12. Wang, Y.J., et al., *A comprehensive review of battery modeling and state estimation approaches for advanced*

battery management systems. Renewable & Sustainable Energy Reviews, 2020. **131**.

13. Locorotondo, E., et al., *Development of a battery real-time state of health diagnosis based on fast impedance measurements.* Journal of Energy Storage, 2021. **38**.
14. Jiang, Y., et al., *State of Health Estimation for Lithium-Ion Battery Using Empirical Degradation and Error Compensation Models.* Ieee Access, 2020. **8**: p. 123858-123868.
15. Yao, H., et al., *Novel Lithium-Ion Battery State-of-Health Estimation Method Using a Genetic Programming Model.* Ieee Access, 2020. **8**: p. 95333-95344.
16. Yun, Z. and W. Qin, *Remaining Useful Life Estimation of Lithium-Ion Batteries Based on Optimal Time Series Health Indicator.* Ieee Access, 2020. **8**: p. 55447-55461.
17. Wang, Y.J., M.C. Li, and Z.H. Chen, *Experimental study of fractional-order models for lithium-ion battery and ultra-capacitor: Modeling, system identification, and validation.* Applied Energy, 2020. **278**.
18. Khayamy, M., A. Nasiri, and O. Okoye, *Development of an Equivalent Circuit for Batteries Based on a Distributed Impedance Network.* Ieee Transactions on Vehicular Technology, 2020. **69**(6): p. 6119-6128.
19. Wang, S., et al., *A novel safety assurance method based on the compound equivalent modeling and iterate reduce particle-adaptive Kalman filtering for the unmanned aerial vehicle lithium ion batteries.* Energy Science & Engineering, 2020. **8**(5): p. 1484-1500.
20. Zhao, T., et al., *A study on half-cell equivalent circuit model of lithium-ion battery based on reference electrode.* International Journal of Energy Research, 2021. **45**(3): p. 4155-4169.
21. Wang, Y.J. and Z.H. Chen, *A framework for state-of-charge and remaining discharge time prediction using unscented particle filter.* Applied Energy, 2020. **260**.
22. Qiao, J., et al., *A novel bias compensation recursive least square-multiple weighted dual extended Kalman filtering method for accurate state-of-charge and state-of-health co-estimation of lithium-ion batteries.* International Journal of Circuit Theory and Applications, 2021.
23. Stroe, D.-I. and E. Schaltz, *Lithium-Ion Battery State-of-Health Estimation Using the Incremental Capacity Analysis Technique.* Ieee Transactions on Industry Applications, 2020. **56**(1): p. 678-685.
24. Xiao, D., et al., *Reduced-Coupling Coestimation of SOC and SOH for Lithium-Ion Batteries Based on Convex Optimization.* Ieee Transactions on Power Electronics, 2020. **35**(11): p. 12332-12346.
25. Shrivastava, P., et al., *Overview of model-based online state-of-charge estimation using Kalman filter family for lithium-ion batteries.* Renewable & Sustainable Energy Reviews, 2019. **113**.
26. Shrivastava, P., et al., *Combined State of Charge and State of Energy Estimation of Lithium-Ion Battery Using Dual Forgetting Factor-Based Adaptive Extended Kalman Filter for Electric Vehicle Applications.* Ieee Transactions on Vehicular Technology, 2021. **70**(2): p. 1200-1215.
27. Locorotondo, E., et al., *Design of a Wireless Charging System for Online Battery Spectroscopy.* Energies, 2021. **14**(1).
28. Liu, Z.X., et al., *Accurate and Efficient Estimation of Lithium-Ion Battery State of Charge with Alternate Adaptive Extended Kalman Filter and Ampere-Hour Counting Methods.* Energies, 2019. **12**(4).
29. Wang, Y., et al., *A State of Charge Estimation Method of Lithium-Ion Battery Based on Fused Open Circuit Voltage Curve.* Applied Sciences-Basel, 2020. **10**(4).
30. Jiang, C., et al., *A state-of-charge estimation method of the power lithium-ion battery in complex conditions based on adaptive square root extended Kalman filter.* Energy, 2021. **219**.
31. Peng, N., et al., *Online parameters identification and state of charge estimation for lithium-ion batteries using improved adaptive dual unscented Kalman filter.* International Journal of Energy Research, 2021. **45**(1): p. 975-990.
32. Ma, L., C. Hu, and F. Cheng, *State of Charge and State of Energy Estimation for Lithium-Ion Batteries Based on a Long Short-Term Memory Neural Network.* Journal of Energy Storage, 2021. **37**: p. 10.
33. Chen, A., et al., *A Temperature and Current Rate Adaptive Model for High-Power Lithium-Titanate Batteries Used in Electric Vehicles.* Ieee Transactions on Industrial Electronics, 2020. **67**(11): p. 9492-9502.

34. Choi, E. and S. Chang, *A Temperature-Dependent State of Charge Estimation Method Including Hysteresis for Lithium-Ion Batteries in Hybrid Electric Vehicles.* Ieee Access, 2020. **8**: p. 129857-129868.
35. Hasan, R. and J. Scott, *Comments on "State of Charge-Dependent Polynomial Equivalent Circuit Modeling for Electrochemical Impedance Spectroscopy of Lithium-Ion Batteries".* Ieee Transactions on Power Electronics, 2020. **35**(4): p. 4448-4448.
36. Ji, Y.-j., S.-l. Qiu, and G. Li, *Simulation of second-order RC equivalent circuit model of lithium battery based on variable resistance and capacitance.* Journal of Central South University, 2020. **27**(9): p. 2606-2613.
37. Pourjafar, S., et al., *A bidirectional multiport DC-DC converter applied for energy storage system with hybrid energy sources.* International Journal of Circuit Theory and Applications, 2021. **49**(8): p. 2453-2478.
38. Moner Al Chawa, M., et al., *Exploring resistive switching-based memristors in the charge-flux domain: A modeling approach.* International Journal of Circuit Theory and Applications, 2018. **46**(1): p. 29-38.
39. Cui, X., et al., *A New Method for State of Charge Estimation of Lithium-Ion Batteries Using Square Root Cubature Kalman Filter.* Energies, 2018. **11**(1).
40. Wang, Y.J., et al., *A fractional-order model-based state estimation approach for lithium-ion battery and ultra-capacitor hybrid power source system considering load trajectory.* Journal of Power Sources, 2020. **449**.
41. Zhang, G., et al., *Hourglass-shaped impedance network based nonelectrolytic capacitors high step-up converter with low voltage stress.* International Journal of Circuit Theory and Applications, 2021. **49**(4): p. 1147-1163.
42. Meng, J.H., et al., *An optimized ensemble learning framework for lithium-ion Battery State of Health estimation in energy storage system.* Energy, 2020. **206**.
43. Meng, J.H., et al., *An Overview and Comparison of Online Implementable SOC Estimation Methods for Lithium-Ion Battery.* Ieee Transactions on Industry Applications, 2018. **54**(2): p. 1583-1591.
44. Jafari, M., et al., *A Novel Predictive Fuzzy Logic-Based Energy Management System for Grid-Connected and Off-Grid Operation of Residential Smart Microgrids.* Ieee Journal of Emerging and Selected Topics in Power Electronics, 2020. **8**(2): p. 1391-1404.
45. Li, P., X. Jiao, and Y. Li, *Adaptive real-time energy management control strategy based on fuzzy inference system for plug-in hybrid electric vehicles.* Control Engineering Practice, 2021. **107**.
46. Sahoo, S.K. and N.K. Kishore, *Battery state-of-charge-based control and frequency regulation in the MMG system using fuzzy logic.* Iet Generation Transmission & Distribution, 2020. **14**(14): p. 2698-2709.
47. Meng, J.H., G.Z. Luo, and F. Gao, *Lithium Polymer Battery State-of-Charge Estimation Based on Adaptive Unscented Kalman Filter and Support Vector Machine.* Ieee Transactions on Power Electronics, 2016. **31**(3): p. 2226-2238.
48. Salama, H.S., et al., *Adaptive Coordination Strategy Based on Fuzzy Control for Electric Vehicles and Superconducting Magnetic Energy Storage-Towards Reliably Operating Utility Grids.* Ieee Access, 2021. **9**: p. 61662-61670.
49. Suhail, M., et al., *Development of Progressive Fuzzy Logic and ANFIS Control for Energy Management of Plug-In Hybrid Electric Vehicle.* Ieee Access, 2021. **9**: p. 62219-62231.
50. Zhang, X., et al., *Fuzzy Adaptive Filtering-Based Energy Management for Hybrid Energy Storage System.* Computer Systems Science and Engineering, 2021. **36**(1): p. 117-130.
51. Kulikov, G.Y. and M.V. Kulikova, *Hyperbolic-singular-value-decomposition-based square-root accurate continuous-discrete extended-unscented Kalman filters for estimating continuous-time stochastic models with discrete measurements.* International Journal of Robust and Nonlinear Control, 2020. **30**(5): p. 2033-2058.
52. Xiong, R., et al., *A Novel Fractional Order Model for State of Charge Estimation in Lithium Ion Batteries.* Ieee Transactions on Vehicular Technology, 2019. **68**(5): p. 4130-4139.

Table 1. The table of fuzzy rule

Δe_k \ e_k (α)	VS	S	M	B	VB
S	VS	VS	S	M	M
M	S	S	M	M	B
B	M	M	M	B	VB
VB	M	M	B	VB	VB

Table 2. Model parameters for the discharging process

SOC(1)	**R_{01}(mΩ)**	**R_1(mΩ)**	**R_2/mΩ**	**C_1(F)**	**C_2(F)**
1	1.626	0.062	0.121	22422.135	145931.520
0.9	1.614	0.083	0.130	22007.309	132337.603
0.8	1.610	0.079	0.158	17419.126	100709.370
0.7	1.605	0.094	0.156	24299.792	173727.939
0.6	1.612	0.070	0.137	21131.495	150309.693
0.5	1.610	0.054	0.108	31975.677	163412.341
0.4	1.624	0.043	0.116	29247.483	129855.272
0.3	1.634	0.042	0.115	33843.308	135943.908
0.2	1.654	0.059	0.118	37889.002	163810.323
0.1	1.683	0.097	0.166	21339.936	144377.786

Table 3. Model parameters for the charging process

SOC(1)	**R_{02}(mΩ)**	**R_1(mΩ)**	**R_2(mΩ)**	**C_1(F)**	**C_2(F)**
0.05	1.631	0.055	0.723	12646.866	18922.522
0.15	1.588	0.041	0.650	18367.969	34076.462
0.25	1.550	0.057	0.572	16758.178	47415.830
0.35	1.535	0.064	0.480	6666.147	38222.889
0.45	1.533	0.066	0.571	11434.338	38551.944
0.55	1.525	0.057	0.669	22566.684	33122.077
0.65	1.501	0.079	0.447	9798.706	35546.444
0.75	1.509	0.065	0.720	10410.944	39177.485
0.85	1.501	0.025	0.346	36210.835	27223.755

Table 4 Comparison of performance indicators of various algorithms under DST operating conditions

Algorithms	**MAE**	**RMSE**
EKF	0.882%	1.146%
CKF	0.860%	1.340%
FASVD-CKF	0.816%	1.276%

Table 5. Comparison of performance indicators of various algorithms under DST operating conditions

Algorithms	**MAE**	**RMSE**
EKF	0.887%	1.181%
CKF	0.864%	1.373%
FASVD-CKF	0.880%	1.380%

Table 6. Comparison of performance indicators of various algorithms under BBDST operating conditions

Algorithms	MAE	RMSE
EKF	0.248%	1.448%
CKF	0.223%	1.326%
FASVD-CKF	0.222%	1.327%

Table 7. Comparison of performance indicators of various algorithms under BBDST operating conditions

Algorithms	MAE	RMSE
EKF	0.966%	1.338%
CKF	0.938%	1.329%
FASVD-CKF	0.941%	1.327%

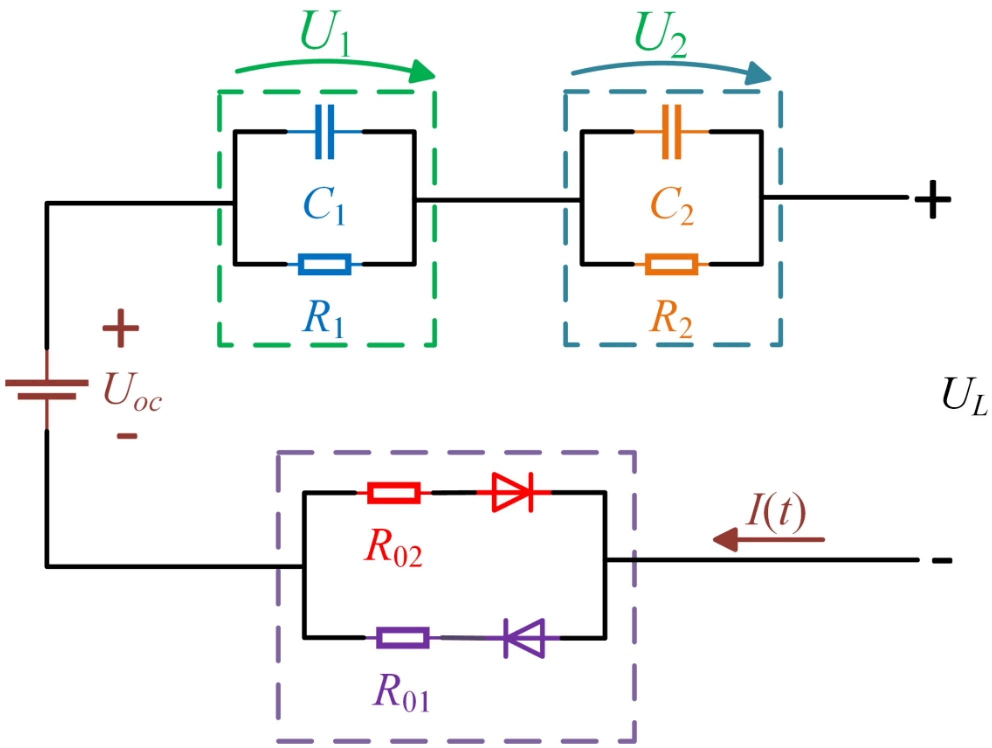

Figure 1. The second-order RC equivalent model of lithium-ion battery with double internal resistance

74x56mm (800 x 800 DPI)

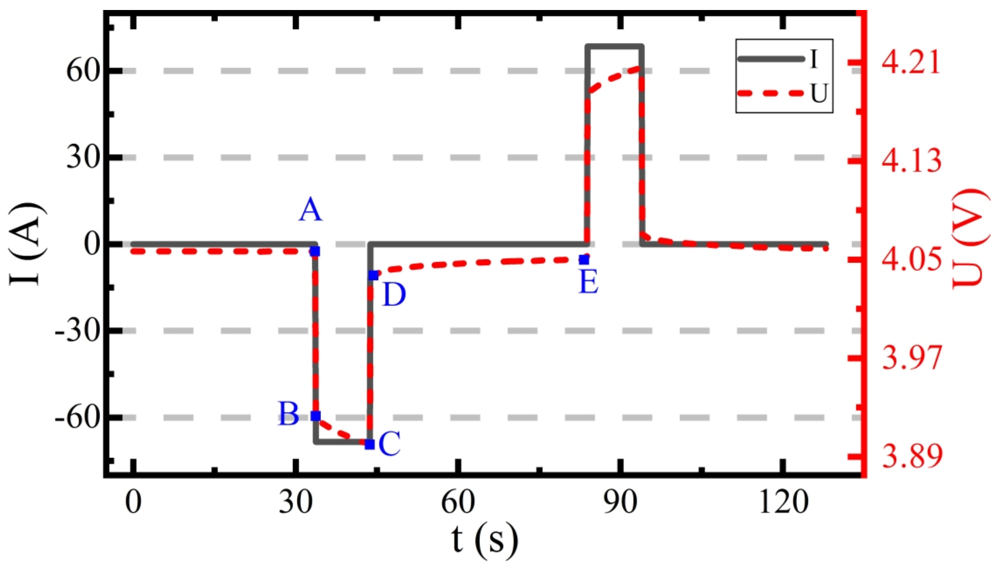

Figure 2. The current and voltage curve of the HPPC working condition

179x99mm (800 x 800 DPI)

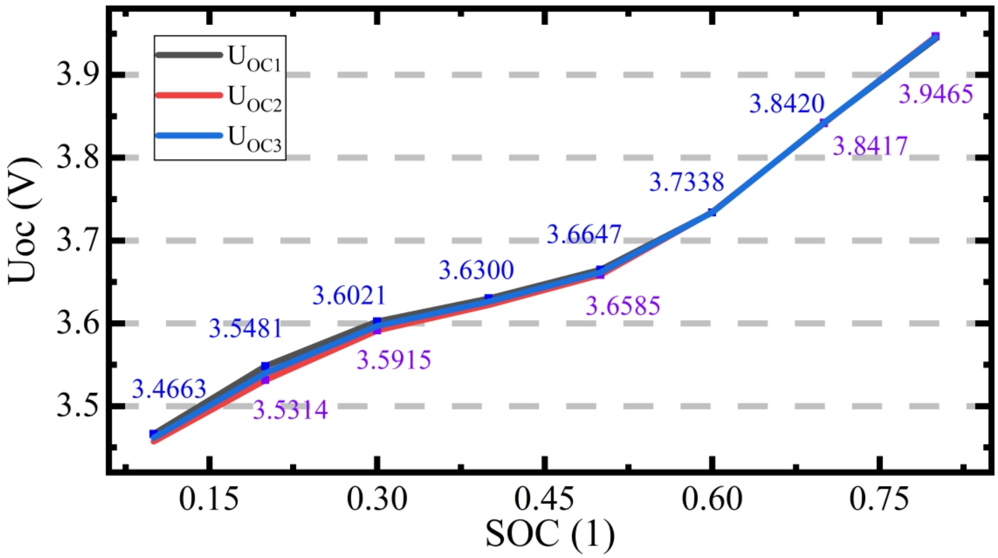

Figure 3. The fitting curve of the UOC-SOC

179x99mm (800 x 800 DPI)

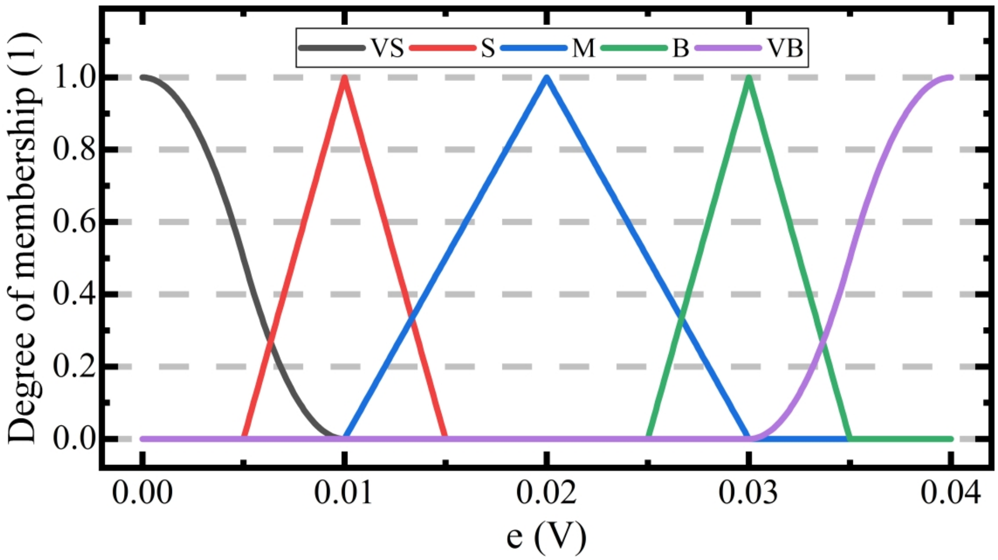

Figure 4 (a). The membership function graph of ek

179x99mm (800 x 800 DPI)

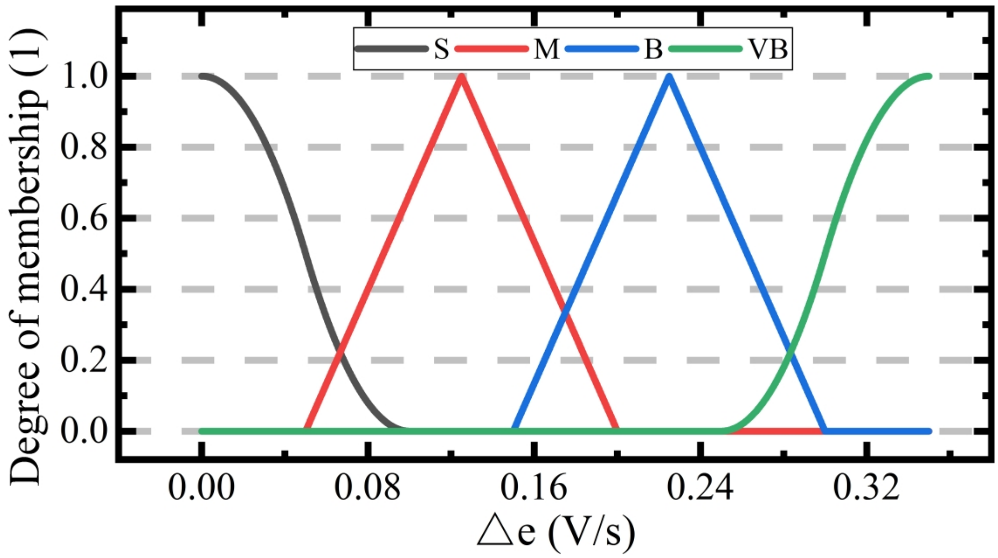

Figure 4 (b).The membership function graph of Δek

179x98mm (800 x 800 DPI)

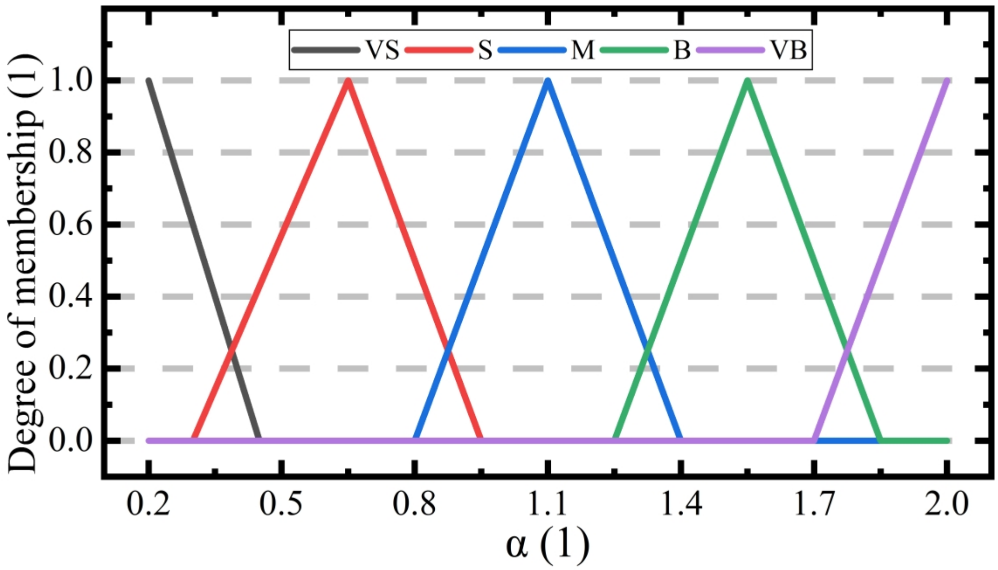

Figure 5. The membership function graph of the output variable

176x99mm (800 x 800 DPI)

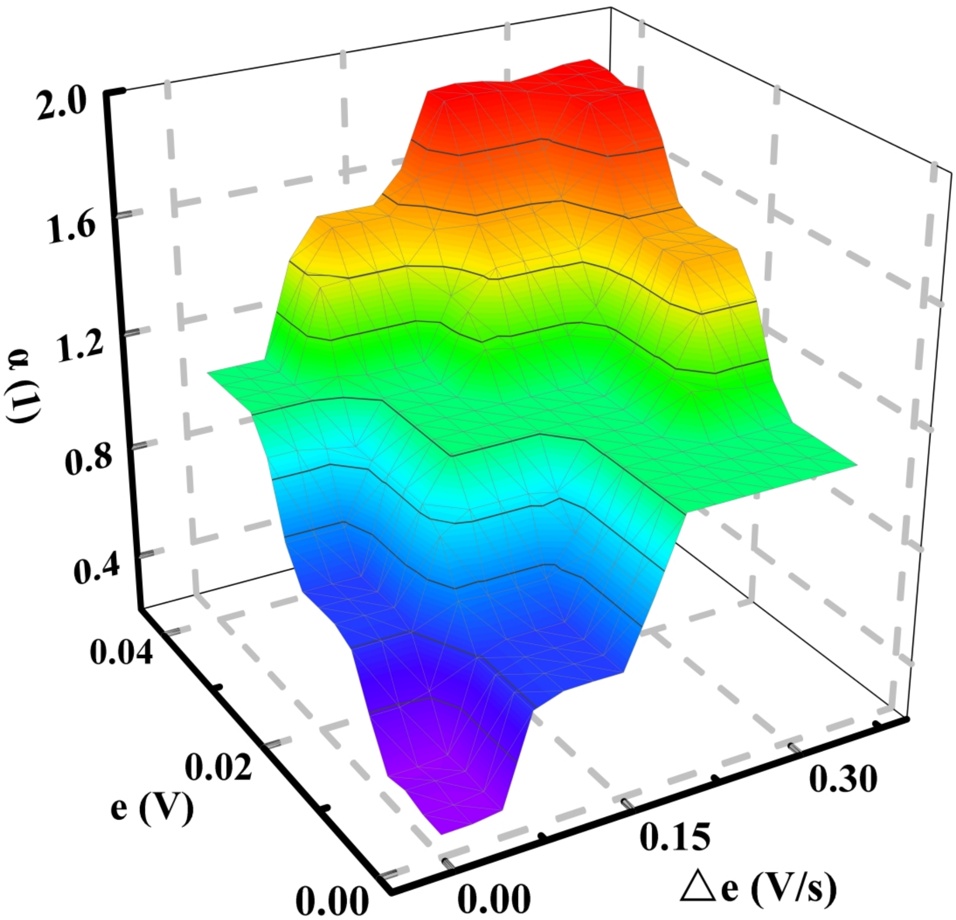

Figure 6. The graph of fuzzy rules

144x134mm (800 x 800 DPI)

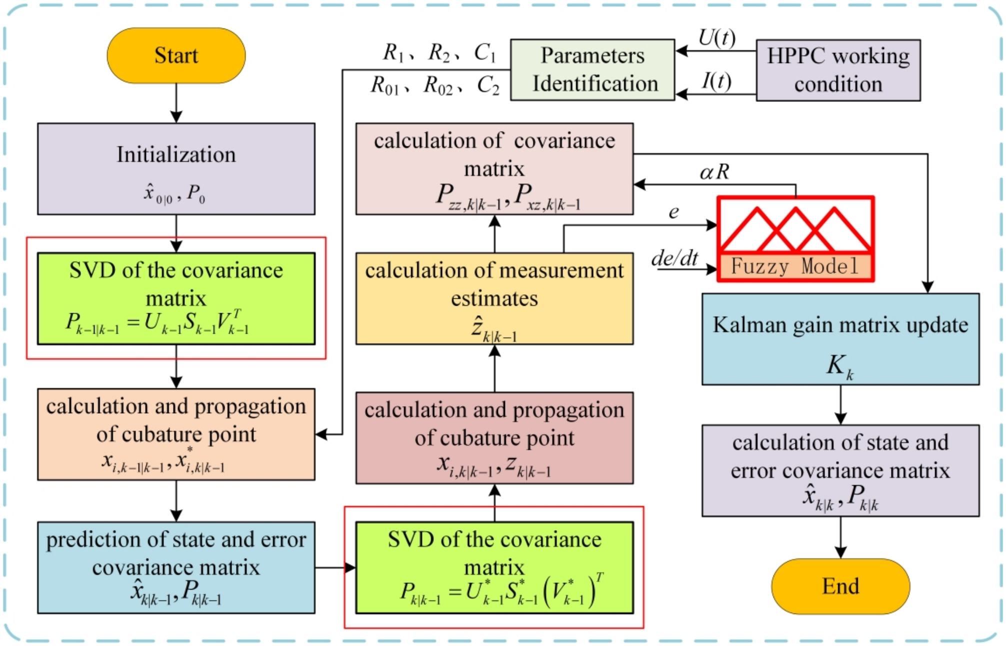

Figure 7. The flow chart of FASVD-CKF

180x115mm (800 x 800 DPI)

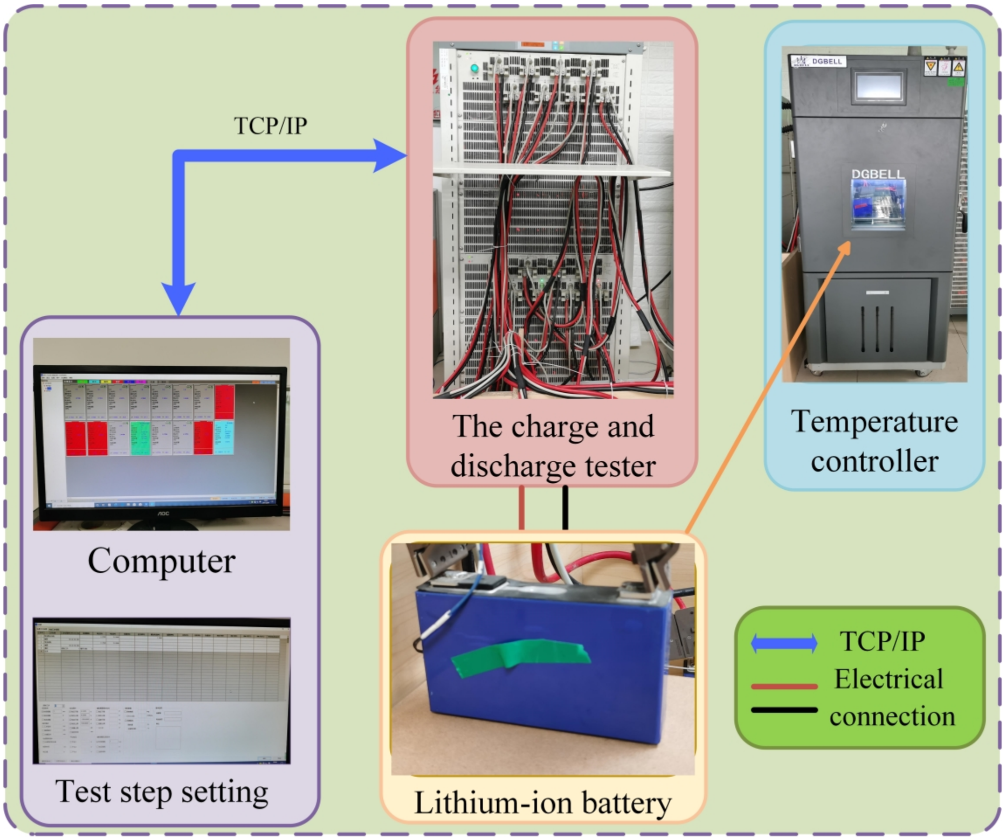

Figure 8. Experimental platform

171x142mm (800 x 800 DPI)

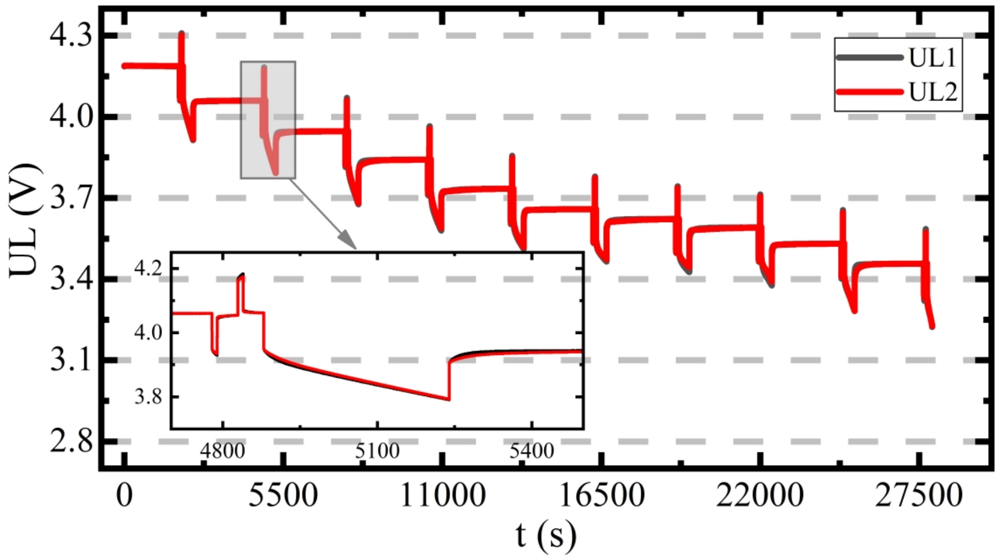

Figure 9 (a).The voltage comparison of HPPC working condition

178x98mm (800 x 800 DPI)

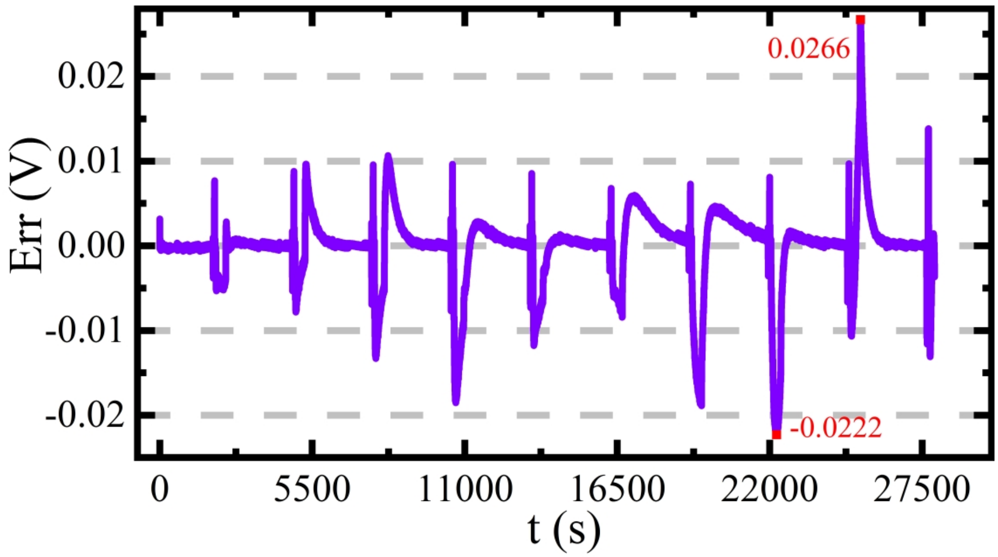

Figure 9 (b). Identification error of HPPC working condition

179x99mm (800 x 800 DPI)

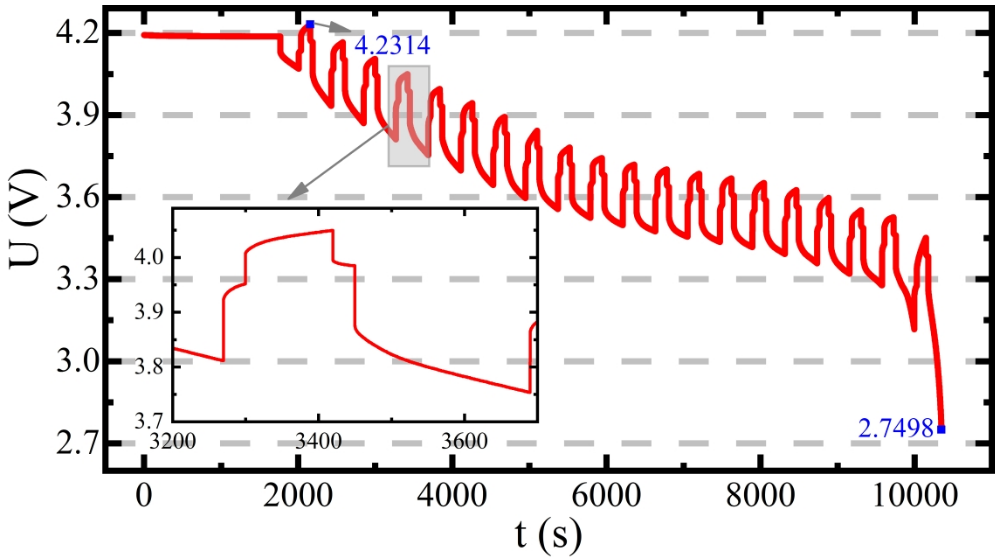

Figure 10 (a).The voltage curve of DST condition

179x99mm (800 x 800 DPI)

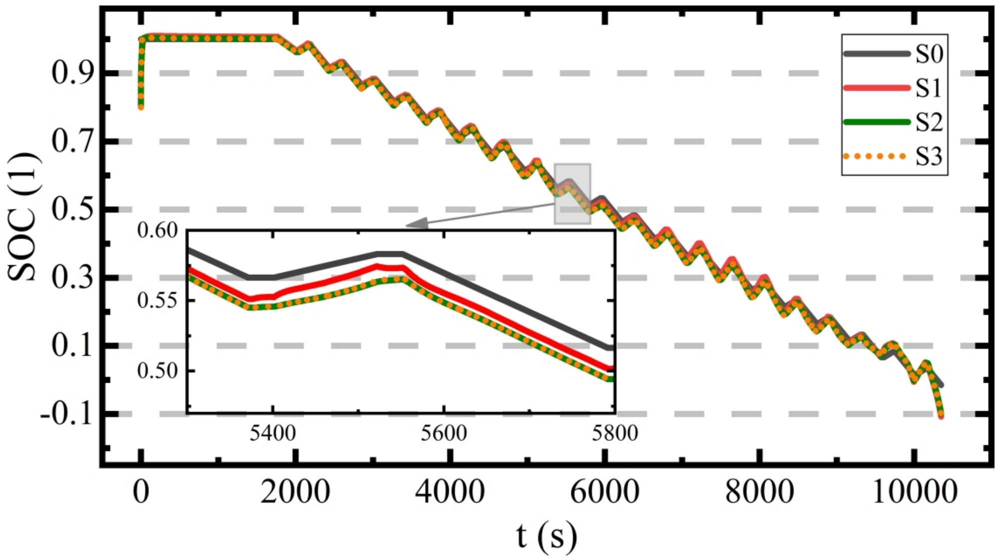

Figure 10 (b). SOC estimation under DST condition

179x99mm (600 x 600 DPI)

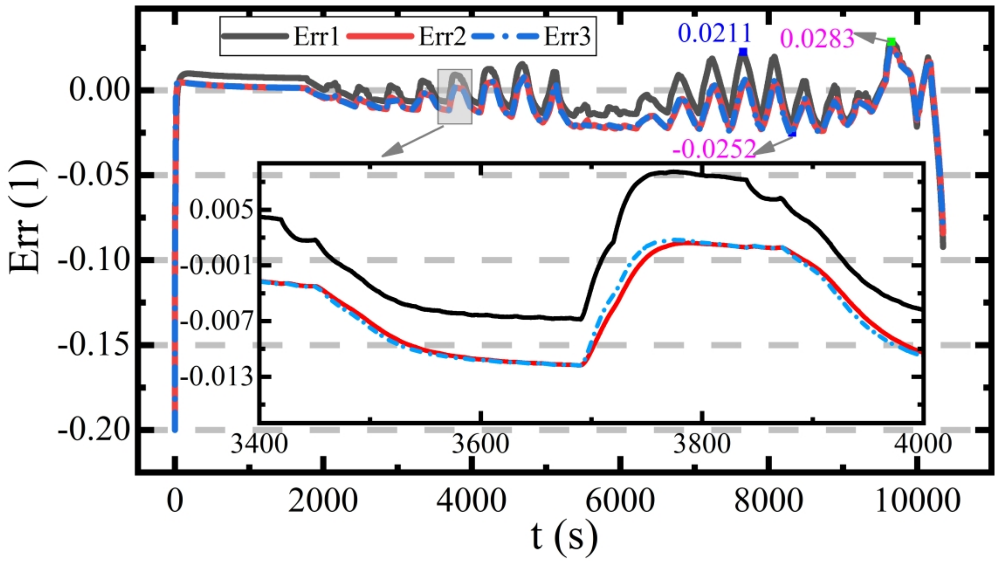

Figure 10 (c). The error of SOC estimation under DST condition

179x99mm (800 x 800 DPI)

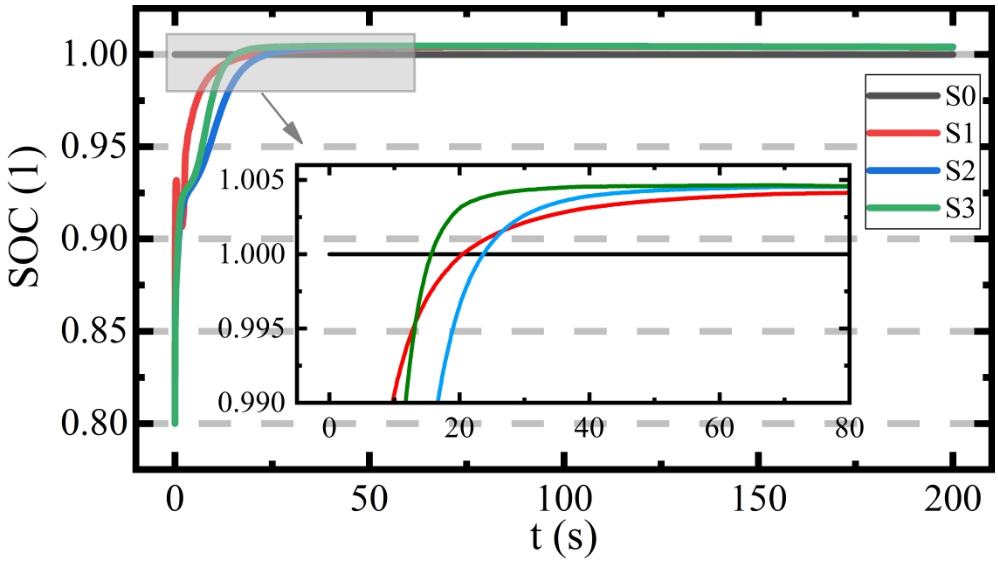

Figure 10 (d). Convergence process of different algorithms under DST condition

181x100mm (800 x 800 DPI)

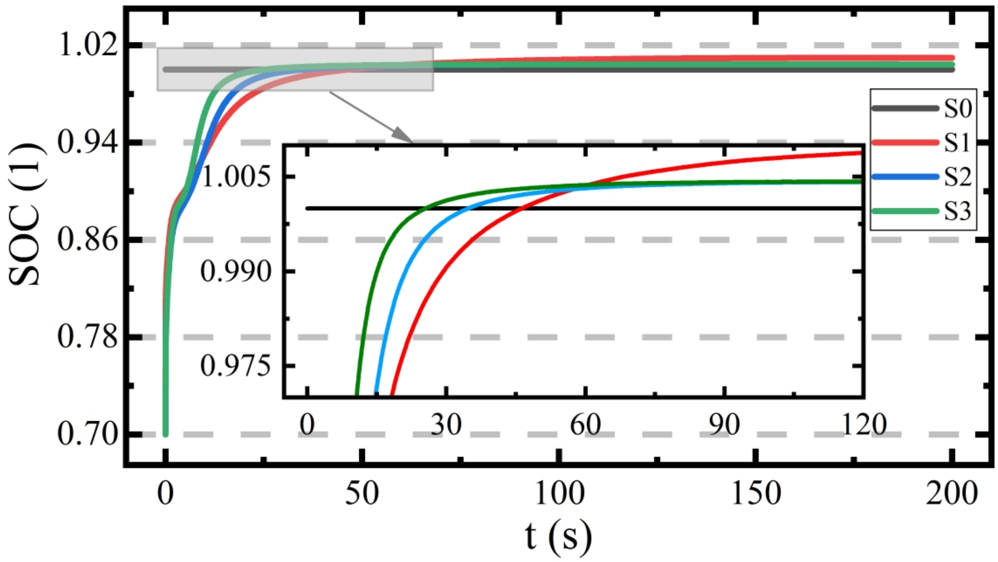

Figure 11 (a).Convergence process of different algorithms under DST

179x99mm (800 x 800 DPI)

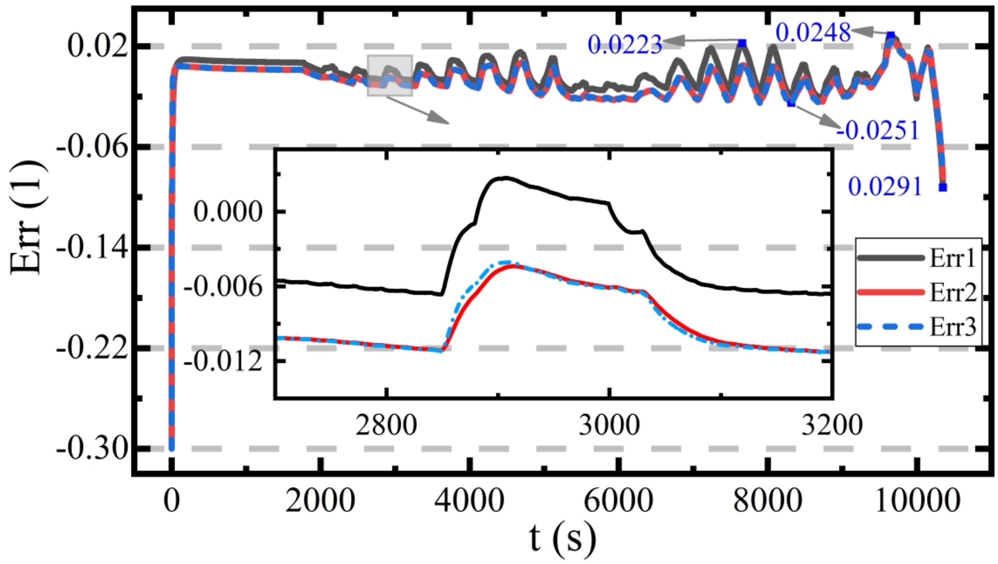

Figure 11 (b).The error of SOC estimation under DST condition

178x99mm (800 x 800 DPI)

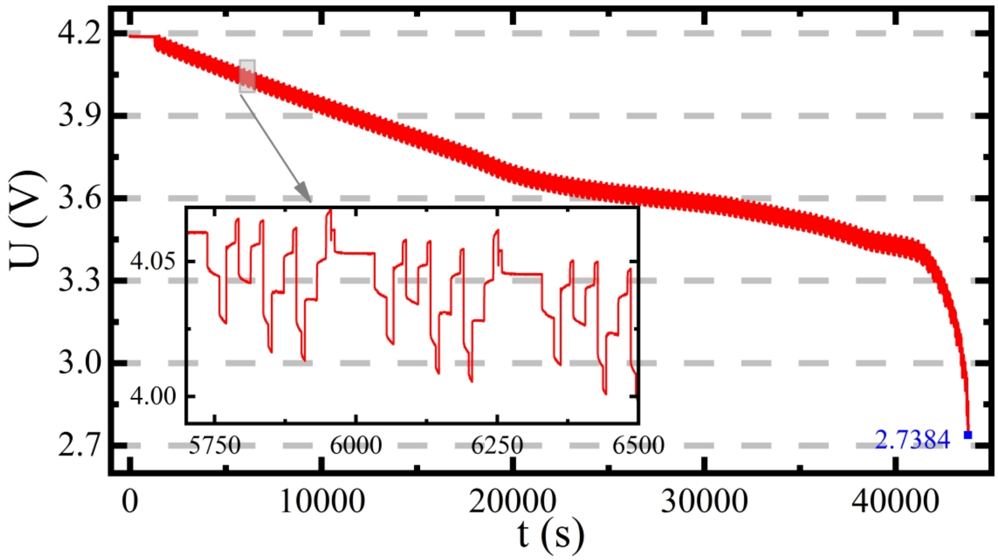

Figure 12 (a). The voltage curve of BBDST condition

179x99mm (800 x 800 DPI)

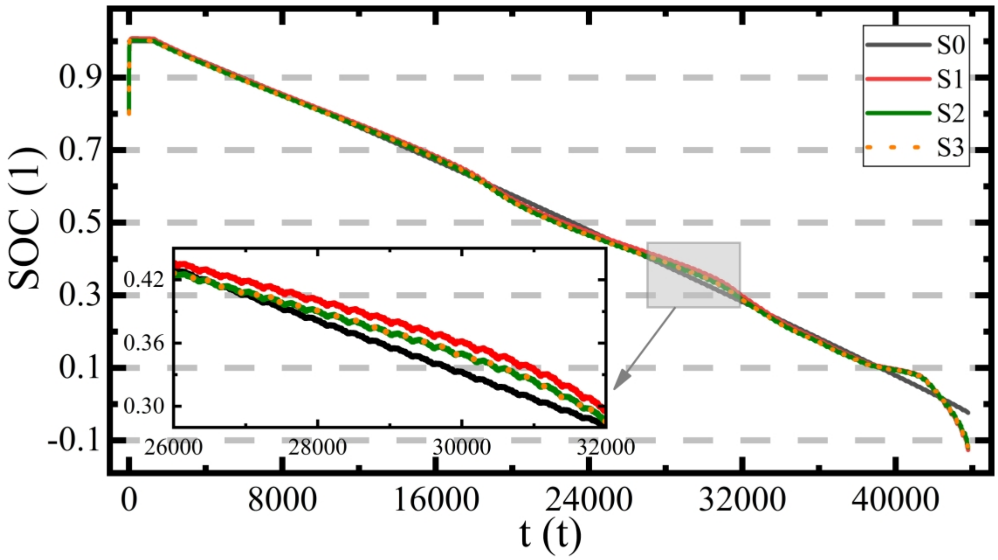

Figure 12 (b). SOC estimation under BBDST condition

179x99mm (600 x 600 DPI)

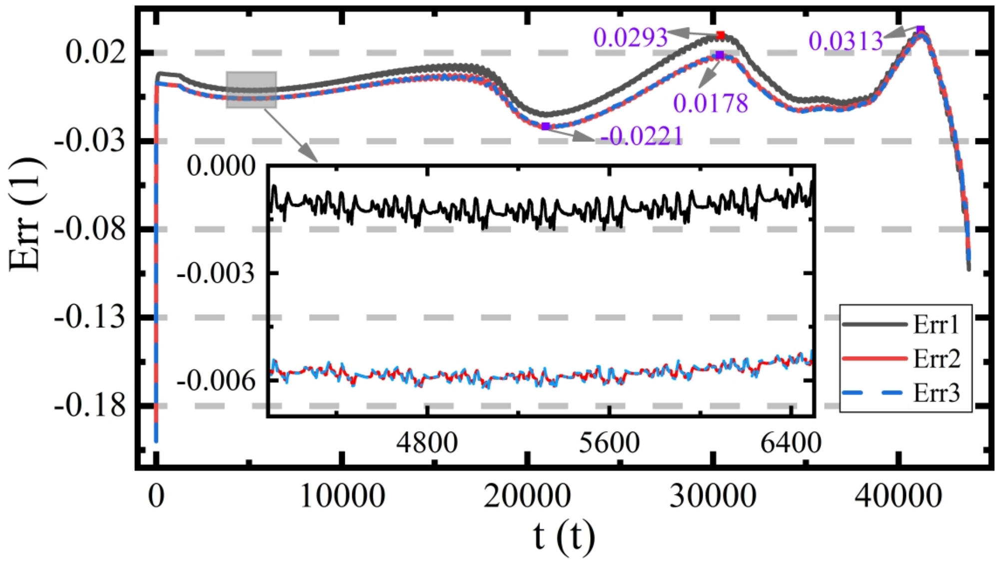

Figure 12 (c). The error of SOC estimation under BBDST condition

179x99mm (800 x 800 DPI)

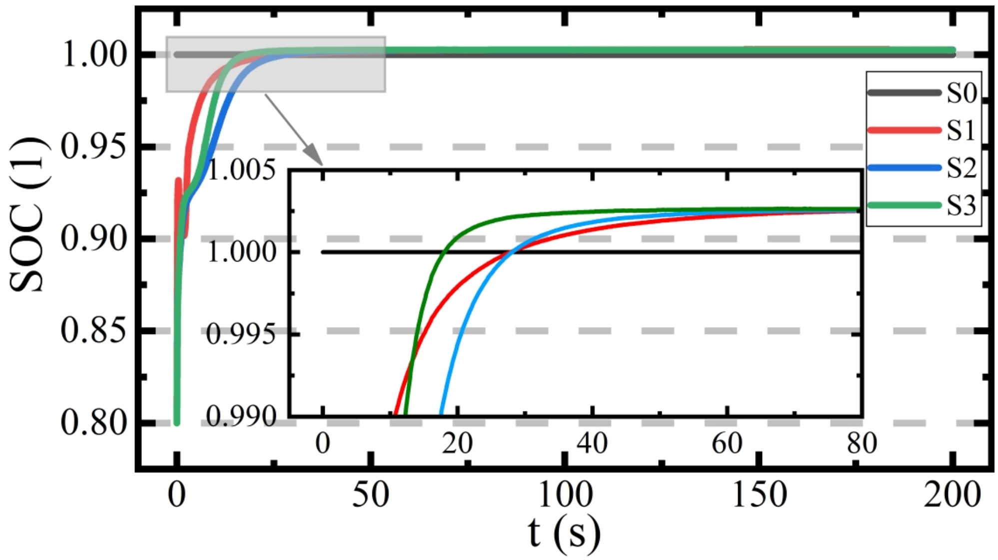

Figure 12 (d). Convergence process of different algorithms under BBDST condition

180x100mm (800 x 800 DPI)

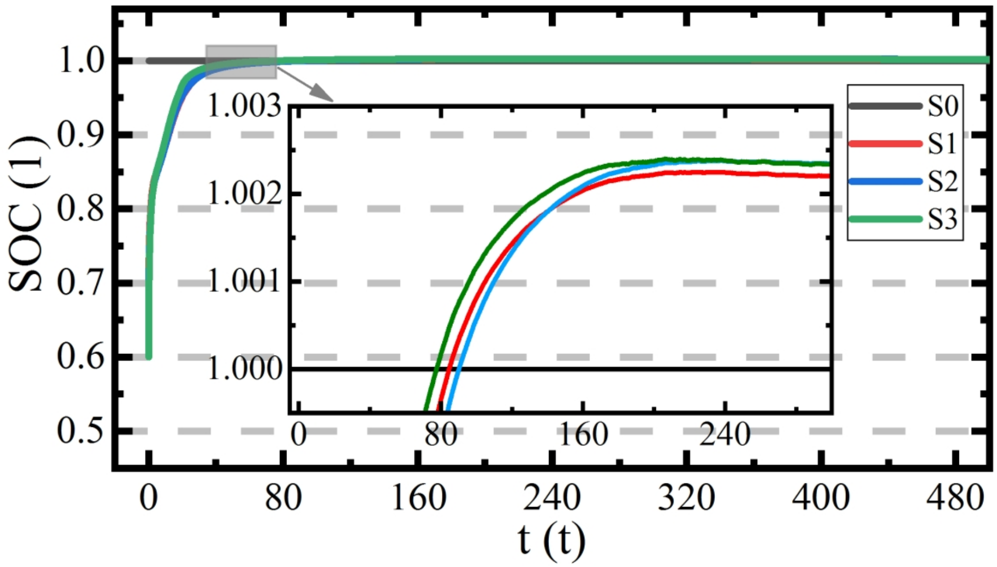

Figure 13 (a). Convergence process of different algorithms under BBDST condition

179x101mm (300 x 300 DPI)

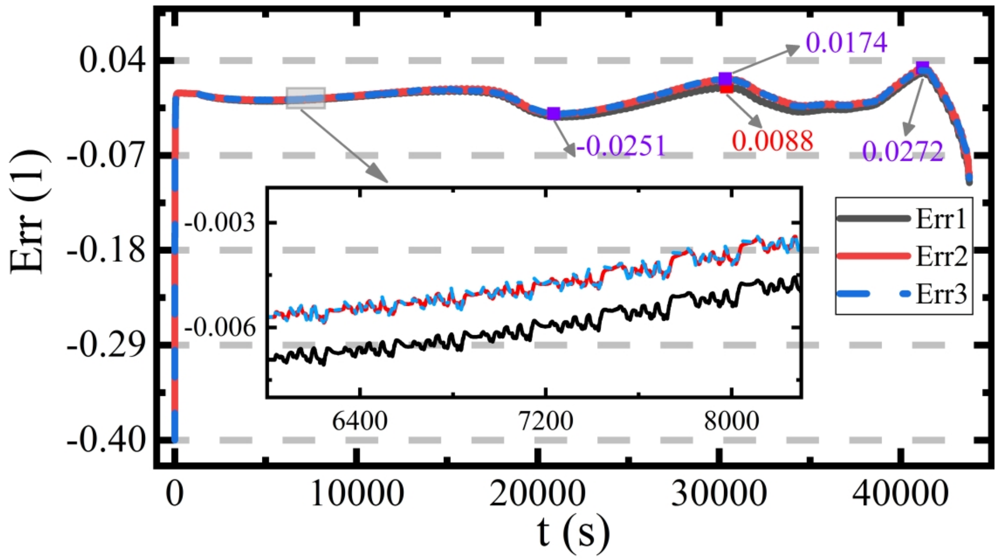

Figure 13 (b). The error of SOC estimation under BBDST condition

180x99mm (800 x 800 DPI)

Fuzzy adaptive singular value decomposition cubature Kalman filtering algorithm for Lithium-ion battery state-of-charge estimation

Xiao Yang[1], Shunli Wang[1*], Wenhua Xu[1], Jialu Qiao[1], Chunmei Yu[1], Carlos Fernandez[2]

[1]School of Information Engineering, Southwest University of Science and Technology, Mianyang 621010, China; [2]School of Pharmacy and Life Sciences, Robert Gordon University, Aberdeen AB10-7GJ, UK.

Abstract: To solve the problem of the slow convergence speed for the battery state-of-charge estimation of cubature Kalman filter algorithm (CKF), a Fuzzy adaptive singular value decomposition cubature Kalman filtering algorithm (FASVD-CKF) is proposed. And a double internal resistance second-order RC model is established to simulate the lithium-ion batteries. Finally, the proposed algorithm is verified under two different working conditions. The results show that the proposed algorithm has fast convergence speed, good stability, and high accuracy in SOC estimation.

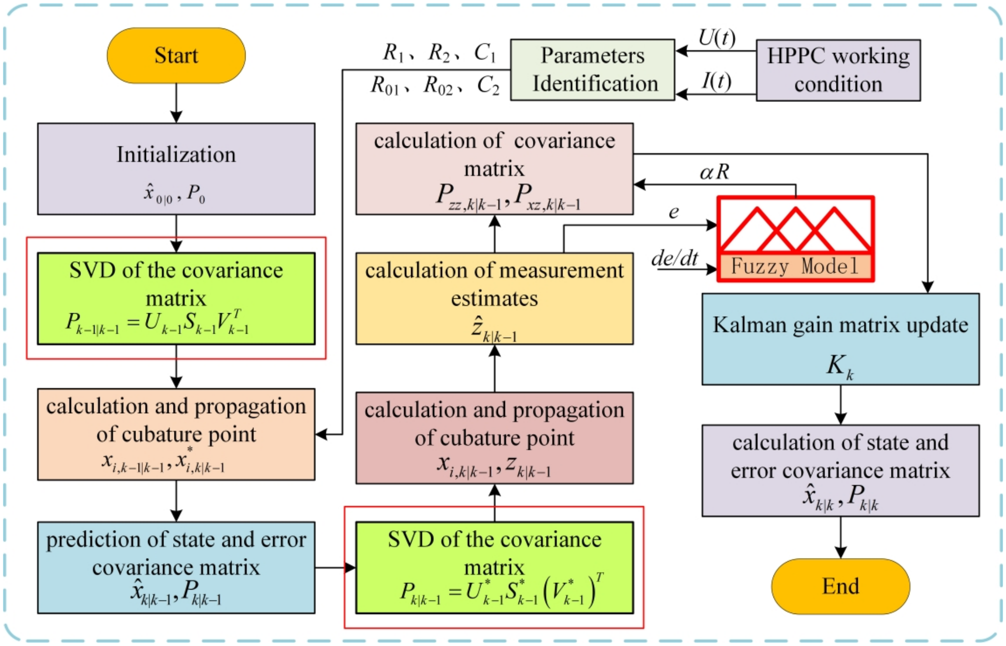

180x115mm (800 x 800 DPI)